Journal of Geophysical Research: Biogeosciences

RESEARCH ARTICLE
10.1029/2018JG004760

Broad Consistency Between Satellite and Vegetation Model Estimates of Net Primary Productivity Across Global and Regional Scales

Laibao Liu[1,2], Shushi Peng[1,2], Amir AghaKouchak[3], Yuanyuan Huang[4], Yan Li[5], Dahe Qin[6], Aili Xie[1,2], and Shuangcheng Li[1,2]

[1]College of Urban and Environmental Sciences, Peking University, Beijing, China, [2]Key Laboratory for Earth Surface Processes of The Ministry of Education, Peking University, Beijing, China, [3]Center for Hydrometeorology and Remote Sensing, Department of Civil and Environmental Engineering, University of California, Irvine, California, USA, [4]Department of Microbiology and Plant Biology, University of Oklahoma, Norman, Oklahoma, USA, [5]Department of Natural Resources and Environmental Sciences, University of Illinois at Urbana-Champaign, Urbana, Illinois, USA, [6]State Key Laboratory of Cryospheric Sciences, Northwest Institute of Eco-Environment and Resources, Chinese Academy of Sciences, Lanzhou, China

Key Points:
- The sign of NPP's response to drought is consistent across satellite-derived NPP and DGVM-derived NPP over most vegetated areas
- The drought sensitivity of satellite-derived NPP and DGVM-derived NPP peaks in semiarid regions globally
- The DGVM-derived NPP is more sensitive to drought than the satellite-derived NPP

Supporting Information:
- Supporting Information S1

Correspondence to:
S. Li,
scli@urban.pku.edu.cn

Citation:
Liu, L., Peng, S., AghaKouchak, A., Huang, Y., Li, Y., Qin, D., et al. (2018). Broad consistency between satellite and vegetation model estimates of net primary productivity across global and regional scales. *Journal of Geophysical Research: Biogeosciences*, *123*, 3603–3616. https://doi.org/10.1029/2018JG004760

Received 20 AUG 2018
Accepted 6 NOV 2018
Accepted article online 20 NOV 2018
Published online 21 DEC 2018

Abstract Drought has the potential to significantly decrease net primary production (NPP). However, the drought sensitivity of NPP remains unclear globally. Here we investigated the response of NPP to drought for the period 1982–2011 using NPP derived from satellite models, eight dynamic global vegetation models (DGVMs), and several drought indices. Our results indicate that the sign of drought response of NPP is consistent across satellites and DGVMs globally. Both the model and satellite data show a unimodal distribution of drought sensitivity across climatic gradients and indicate that semiarid regions are the most drought-sensitive areas. In addition, a decreasing drought trend was significantly correlated with an increasing trend in satellite-derived NPP or DGVM-derived NPP globally. However, the DGVM-derived NPP is more sensitive to drought than the satellite-derived NPP over most vegetated land areas and presents a stronger correlation with drought, higher drought sensitivity, and larger slopes between NPP and drought trends. The overresponse of the DGVM-derived NPP to drought relative to the satellite-derived NPP could be attributed to the higher drought sensitivity of the simulated leaf area index and overresponse of the DGVM-derived NPP to the vapor pressure deficit. Overall, large uncertainties remain in the response of NPP to drought and additional long-term observations are required to better represent NPP responses to water stress in DGVM models.

1. Introduction

Terrestrial net primary production (NPP) is the net carbon gain by vegetation, that is, the difference between gross primary production and autotrophic respiration, providing important ecosystem services of climate change mitigation. From a social perspective, NPP is a source of food, biofuel, and fiber worldwide and supports the survival of human beings (Haberl et al., 2007; Running, 2012; Smith et al., 2012). Because of the importance of NPP for human well-being, considerable efforts have been made to estimate global terrestrial NPP and its changes using satellite observations and terrestrial ecosystem models (Field et al., 1998; Nemani et al., 2003; Sitch et al., 2008; Smith et al., 2016; Zhao & Running, 2010). In the context of global change, it is essential to better understand and predict changes in NPP (Running, 2012).

The changes of NPP are generally controlled by climate, in particular by precipitation, temperature, and solar radiation (Nemani et al., 2003). In addition, CO_2 and nutrient fertilization (Norby et al., 2010; Schimel et al., 2015; Sitch et al., 2008) and short-term natural and anthropogenic disturbances (e.g., fires, logging, infestations) can influence the vegetation growth at various spatiotemporal scales (Le Quéré et al., 2016). Recent studies suggest that extreme events, such as drought, heat waves, or storms, and the associated disturbances can cause large negative impacts on NPP and even bring ecosystems to a tipping point for collapse (Anderegg et al., 2015; Ciais et al., 2005; Reichstein et al., 2013). Yet there remain large uncertainties in the characterization of changes in NPP trigged by climate extremes (Frank et al., 2015; Powell et al., 2013). Thus, to obtain reliable estimates of the sign and magnitude of changes in terrestrial NPP and reliable

assessments of food safety and bioenergy, a better understanding of both the occurrence of climate extremes themselves and their impacts on NPP needs to be achieved (Reichstein et al., 2013).

Water availability is the most limiting factor for vegetation growth globally (Nemani et al., 2003). Water-related climate extremes, such as drought, are reported to have the strongest and most extensive effects on terrestrial NPP among all climate extremes (Frank et al., 2015; Zscheischler et al., 2013). Terrestrial ecosystem models are widely used to quantify and project NPP responses to historical and future drought (Hoover & Rogers, 2016; Jiang et al., 2013; Reichstein et al., 2013), but large uncertainties remain regarding the response of NPP to drought in models (AghaKouchak et al., 2015; Huang et al., 2016; Powell et al., 2013; Wang et al., 2012). For example, Powell et al. (2013) found that five terrestrial biosphere models poorly simulated the carbon and water fluxes under imposed drought in the Amazon. Piao et al. (2013) also showed an overresponse of gross primary productivity (GPP) to precipitation from ten terrestrial ecosystem models. However, the ability of terrestrial ecosystem models to simulate the response of NPP to drought remains relatively unknown on a global scale and needs additional analyses. Besides, a recent study highlighted that the drought sensitivity of ecosystem productivity peaked in semiarid regions across southeastern Australia based on the satellite-derived vegetation index (Ma et al., 2015). This is of great interest, because semiarid regions cover approximately 40% of the global land areas. But it is not known that whether the regional results can be extrapolated to the global scale and whether terrestrial ecosystem model can reproduce the high drought sensitivity of semiarid regions. Recently, long-term satellite-based NPP products have become available, such as satellite-derived NPP (Smith et al., 2016), and they have enabled evaluations of the regional and global impacts of drought over the past three decades. For instance, Liu et al. (2017) used this satellite NPP product to evaluate the seasonal responses of terrestrial NPP to climate variation in the Coupled Model Intercomparison Project phase 5 (CMIP5) models.

In this study, we derived NPP from satellite models and simulated NPP using eight dynamic global vegetation models (DGVMs). We used the historical Standardized Precipitation Evapotranspiration Index (SPEI) and self-calibrating Palmer Drought Severity Index (scPDSI) to characterize drought stress. We aimed to address the following questions: (1) Are there any substantial discrepancies in the drought response between DGVM-derived NPP and satellite-derived NPP? If there is a large difference, what is the underlying mechanism? (2) Whether semi-arid regions are most sensitive to drought on a global scale?

2. Materials and Methods

2.1. Satellite Models

All data used in this study span the period from 1982 to 2011. Global monthly satellite-derived NPP data with 0.5° spatial resolution were obtained from Smith et al. (2016). This satellite NPP data were calculated using the Moderate Resolution Imaging Spectroradiometer (MODIS) NPP algorithm based on the third-generation Global Inventory Modeling and Mapping Studies Fraction of Absorbed Photosynthetically Active Radiation (FAPAR), Global Inventory Modeling and Mapping Studies-derived Leaf Area Index (LAI) data (http://sites.bu.edu/cliveg/; Zhu et al., 2013), and climate data (National Centers for Environmental Prediction (NCEP)–Department of Energy Reanalysis; http://www.esrl.noaa.gov). The MODIS NPP algorithm, FAPAR, and LAI data sets have been extensively evaluated against a large amount of observational data, and they are capable of realistically monitoring vegetation production across different biome types globally (Running et al., 2004; Zhu et al., 2013).

Additionally, the biweekly third-generation Normalized Difference Vegetation Index (NDVI3g) data of 1982–2011 with a 0.083° spatial resolution were also used as a proxy of vegetation productivity, which was obtained from the Global Inventory Modeling and Mapping Studies group (https://ecocast.arc.nasa.gov/data/pub/gimms/3g.v1/; Tucker et al., 2005). This product has been carefully processed to remove several detrimental effects, including calibration loss, orbit drift, and volcanic eruption. The biweekly GIMSS-NDVI series were composited monthly based on maximum monthly value. They were further aggregated to 0.5° to match the resolution of satellite NPP using the bilinear interpolation.

2.2. Dynamic Global Vegetation Models

The NPP and LAI data sets simulated from the latest version of Trends in net land carbon exchange (TRENDY-V5; http://dgvm.ceh.ac.uk/node/9/) of 1982–2011 were used (Sitch et al., 2015). The models used in this study

are listed in Table S1 (Barman et al., 2014; El-Masri et al., 2013; Lawrence et al., 2011; Oleson et al., 2010; Raddatz et al., 2007; Smith et al., 2001; Stocker et al., 2013; Wang et al., 2010, 2011; Zeng et al., 2005). Each model was run with the S2 scenario, which accounts for climate change and rising atmospheric CO_2 concentrations but does not account for land use change. Simulations are forced with climate data from CRU-NCEP v7 (http://dods.extra.cea.fr/data/p529viov/cruncep). CRU-NCEP v7 is a merged product of Climate Research Unit (CRU TS3.24) observation-based monthly 0.5° climate variables (http://www.cru.uea.ac.uk/) and the NCEP reanalysis. All simulations were aggregated into a 0.5° using the bilinear interpolation. The ensemble mean of DGVM outputs consists of results from eight models (Table S1). All satellite-derived data sets and DGVM outputs have been widely used to evaluate terrestrial ecosystem production (Jung et al., 2017; Peng et al., 2013).

2.3. Drought Indices

2.3.1. Standardized Precipitation Evapotranspiration Index

The SPEI calculated using monthly precipitation and potential evapotranspiration (PET) was used to characterize drought severity, with low values indicating drier conditions, whereas high values indicating wetter conditions (Beguería et al., 2014; Vicente-Serrano et al., 2010). The SPEI V2.4 data set with a 0.5° spatial resolution and monthly temporal resolution used in this study was obtained from the digital Institutional Repository of the Spanish National Research Council (http://spei.csic.es/index.html). Monthly precipitation and PET were derived from the CRU TS 3.23. SPEI considers the surface water balance by accounting for differences between precipitation and evapotranspiration at different time scales. In particular, the PET in this version was calculated using the more sophistical Penman-Monteith method. A time scale of three months is commonly used in drought assessment (Huang et al., 2016; Zscheischler et al., 2014); thus, the three-month SPEI (hereafter SPEI3) was used in the main results. A six-month SPEI (hereafter SPEI6) was also used to verify the robustness of our results.

2.3.2. Self-Calibrating Palmer Drought Severity Index

To test the robustness of our results, we also used the Self-calibrating Palmer Drought Severity Index (scPDSI), which was calculated using CRU TS 3.25 climate data and could be obtained from the CRU (Schrier et al., 2013). A lower scPDSI generally implies a drier climate. The PET calculations in this data set used the Penman-Monteith method. This product has a spatial resolution of 0.5° and a monthly temporal resolution.

2.4. Aridity Index

The aridity index is defined as the ratio of precipitation to PET. Monthly precipitation and PET with a 0.5° spatial resolution were derived from the CRU (Harris et al., 2014). The classification standard introduced by UNESCO is provided in Table S2 (UNESCO, 1979). Because tropical forests have unique climate conditions, we separated these areas from humid regions. The tropical forest classification is based on a MODIS land cover classification (MCD12C1, type3; https://lpdaac.usgs.gov/data_access/data_pool) and the Köppen-Geiger classification (Peel et al., 2007), following Ahlström et al. (2015) (Figure 1). Thus, regionally, the global land areas are divided into six climatic regions: hyperarid, arid, semiarid, subhumid, extratropical humid, and tropical forest.

2.5. Vapor Pressure Deficit

Vapor pressure deficit (VPD) measures the difference between the saturated vapor pressure at air temperature and actual air vapor pressure. Thus, the VPD can indicate moisture stress on vegetation growth (Eamus et al., 2013). The VPD has a 0.5° spatial resolution and was calculated using the maximum temperature, minimum temperature, and vapor pressure derived from the CRU based on the method used by Zhao and Running (2010).

2.6. Statistical Analyses

This study covered global vegetated areas and the study period was 1982–2011 because of the availability of data sets. Regions with sparse vegetation were excluded based on the class of barren or sparsely vegetated in the IGBP land cover classification (MCD12C1, type 1). Monthly drought indices (i.e., three-month SPEI, six-month SPEI, and scPDSI) were averaged to characterize the annual drought severity. Monthly NPP was integrated into annual NPP.

To investigate the response of NPP to drought, Pearson correlation coefficients were calculated to quantify the interannual relationship between annual NPP and annual drought severity. The drought sensitivity of

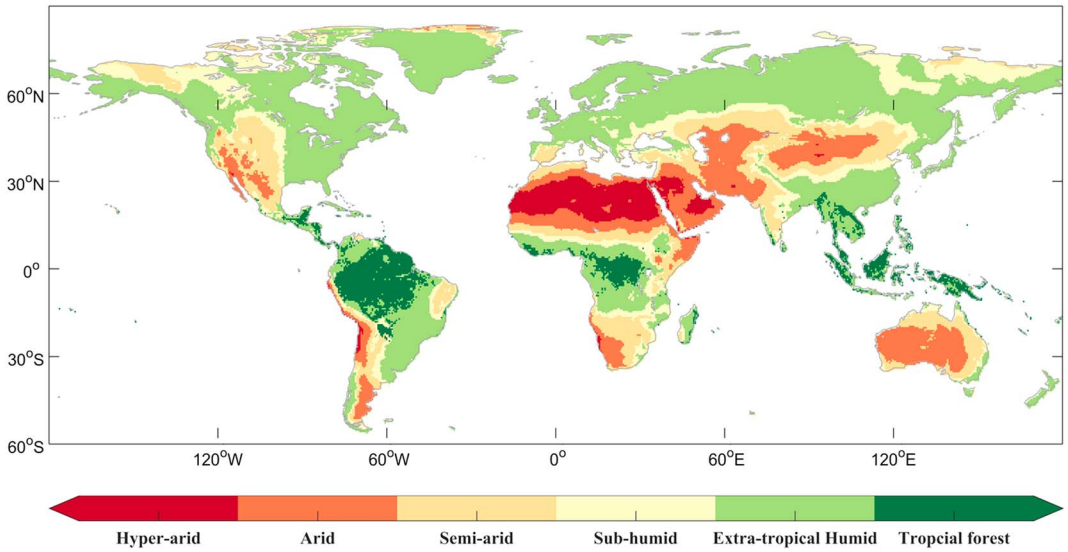

Figure 1. Classification of six climatic regions: hyperarid, arid, semiarid, subhumid, extratropical humid, and tropical forest.

NPP was defined as the change in annual NPP per unit change in annual drought severity. This is equivalent to the slope of the linear regression between annual NPP and annual drought severity. Before computing the correlation coefficients and drought sensitivity, time series data are detrended by subtracting the long-term linear trends to avoid spurious correlations resulting from trends or other confounding variables. We further calculated the drought sensitivity of LAI and the sensitivity of NPP to VPD to help understand the drought sensitivity of NPP. Furthermore, to investigate the driving force of drought trends for the annual NPP trends during 1982–2011, we also calculated the linear regression between NPP trends and annual drought severity trends. The trend of NPP or annual drought severity was the slope of the linear regression between annual NPP or annual drought severity and time. Using a similar method, we also used the FAPAR and NDVI as proxies of vegetation productivity (NPP) to test the robustness of our results.

3. Results

3.1. Changes in NPP From 1982 to 2011

Globally, the multiyear averaged terrestrial NPP estimated from satellite models (NPP_S) and DGVM ensemble mean (NPP_M) from 1982 to 2011 are 50.4 ± 2.9 and 51.4 ± 5.9 PgC/year, respectively. Similar spatial patterns of multiyear average NPP_S and NPP_M were also observed (Figure S1). Spatially, the NPP_S and NPP_M increased over 73.7 and 83.2% of the vegetated land areas, respectively, during 1982–2011 (Figure 2). The regions with the increasing trends, consistent across the two data sets, are in the eastern North America, Europe, North Asia, and southern China. Consistent decreasing trends of NPP are found in the northern China and southern Australia. However, the NPP trends diverge between the NPP_S and NPP_M in the northern South America, and Southeast Asia. In addition, the NPP_M shows larger increasing trends than the NPP_S over most vegetated land areas. Globally, the NPP_S increased by 1.5 ± 0.9 PgC/year (2.8 ± 1.6%), while the NPP_M significantly increased at a threefold rate of 4.9 ± 1.7 PgC/year (9.6 ± 2.5%) from 1982 to 2011. Both the NPP_S and NPP_M show the maximum increases in tropical forests at 0.9 ± 0.4 PgC/year (3.7 ± 1.7%) and 2.6 ± 1 PgC/year (8.9 ± 2.5%), respectively. Additionally, during this period, both the NPP_S and NPP_M decrease in arid regions by 0.03 ± 0.9 PgC/year (3 ± 0.8%) and 0.1 ± 0.9 PgC/year (12 ± 8%), respectively.

3.2. Changes in Annual Drought Severity From 1982 to 2011

Globally, 38.7% of the vegetated land areas have experienced decreasing annual SPEI3 for 1982–2011, and 4.4% of the vegetated land areas were statistically significant at the 0.05 level (Figure 3). Prominent decreasing SPEI3 trends (i.e., more dry) occurred over the southern North America, southern South America, and China. In contrast, increasing trends in SPEI3 (i.e., less dry) were observed over the Northeast Asia, Southeast Asia, the Amazon basin, and Africa. Similar spatial patterns in the scPDSI trends were also observed

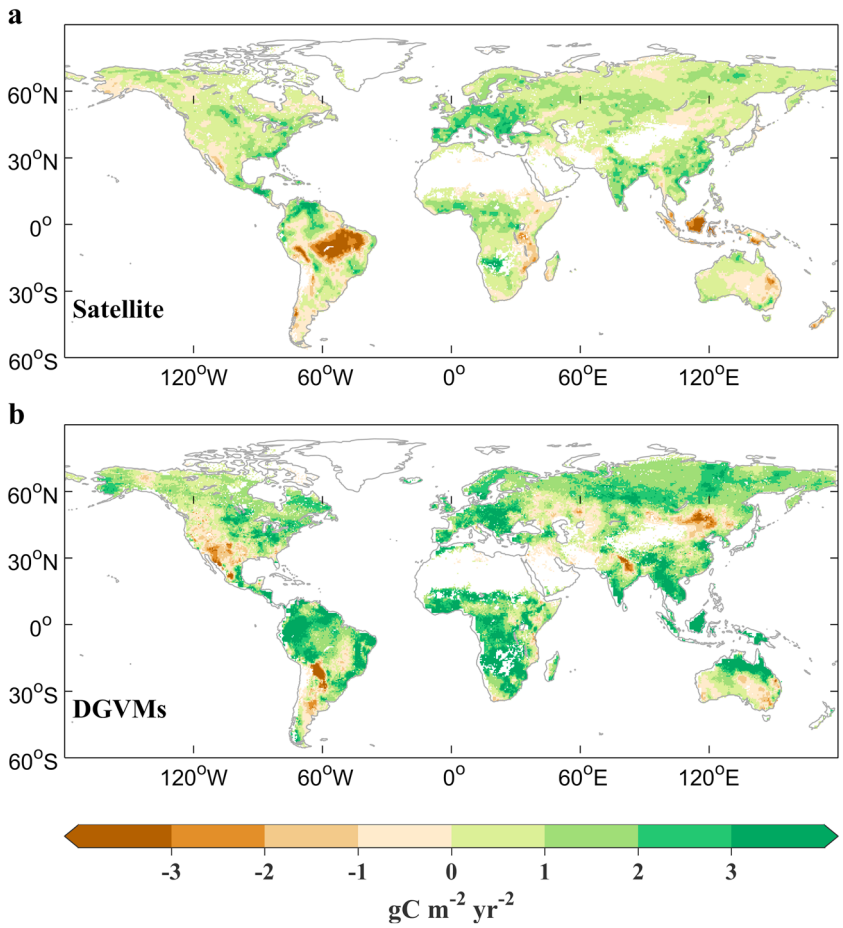

Figure 2. Spatial distributions of the trends in annual NPP from (a) satellite model (NPP_S) and (b) DGVM ensemble mean (NPP_M). Regions with sparse vegetation were masked in white.

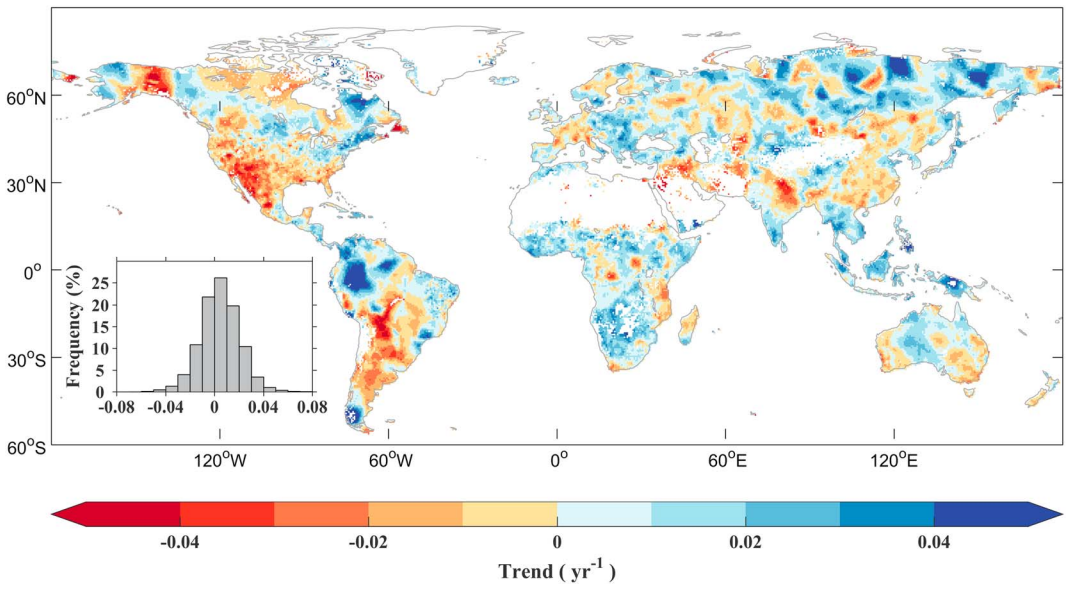

Figure 3. Spatial distribution of the trends in the annual average of the 3-monthly SPEI for 1982–2011. Regions with sparse vegetation were masked in white. The inset in the bottom left corner shows the histogram of the frequency distribution of the SPEI trends.

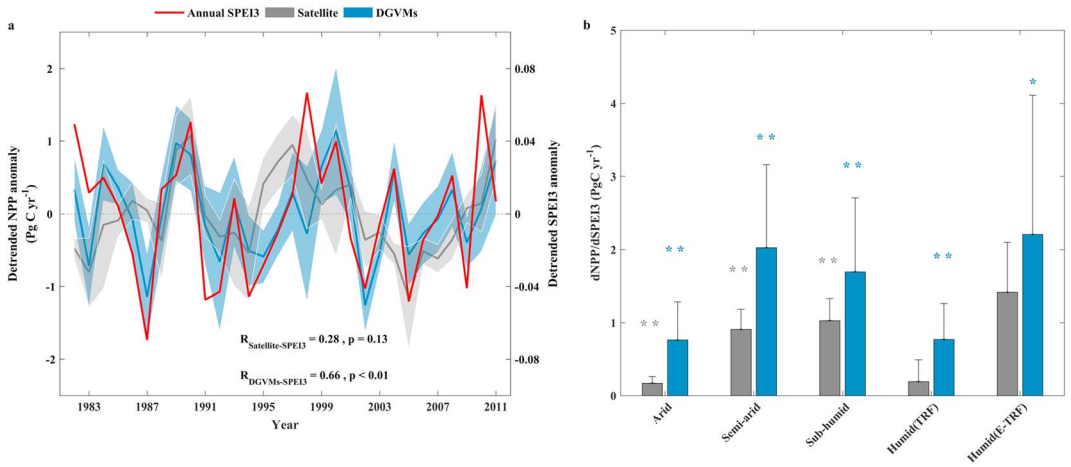

Figure 4. (a) Interannual variations in the detrended annual SPEI3 anomalies (red) and detrended NPP_S anomalies (gray) or NPP_M anomalies (blue) during 1982 to 2011 globally. The shaded area indicates uncertainty (one standard deviation) caused by intermodel variability for the DGVMs and model parameterization for the satellite estimates. The correlation coefficient (R) value shows the interannual correlation coefficients between the SPEI3 and NPP_S (gray) or NPP_M (blue). (b) Sensitivity of the NPP to SPEI3 during 1982–2011 in five individual climatic regions, respectively. Error bars indicate the standard deviation of the sensitivity derived from the satellite data and model simulations. $^{**}p < 0.01$, $^{*}p < 0.05$. dNPP/dSPEI3 without an asterisk are not statistically significant ($p > 0.05$).

from 1982 to 2012 (Figure S2). Globally, the SPEI3 exhibits a significantly increasing trend at a rate of 0.031 decade^{-1} ($p < 0.001$) during 1982–2011. Regionally, the SPEI3 tended to show larger increasing trends in wetter regions. For instance, tropical forests showed the highest increase of SPEI3 (0.1 decade^{-1}) and the smallest fraction of drying area (26.5%), while arid regions experienced the lowest increase of SPEI3 (0.0038 decade^{-1}) and the largest fraction of drying area (46.2%) during 1982–2011.

3.3. Spatial Relationship Between NPP and Drought

From 1982 to 2011, the SPEI3 was positively and significantly correlated with the global NPP_M ($R = 0.66$, $p < 0.01$) but not with the global NPP_S ($R = 0.28$, $p = 0.13$; Figure 4a). Additionally, the NPP_M has a positive apparent sensitivity to the SPEI3 (11.4 ± 6.1 PgC/year or 21.2 ± 8.3% per year), which is approximately 2.5 times larger than the corresponding drought sensitivity of the NPP_S (4.5 ± 2 PgC/year or 8.6 ± 3.8% per year). Regionally, in arid, semiarid, and subhumid regions, both the NPP_M and NPP_S are significantly and positively correlated with the SPEI3 ($p < 0.05$), although the drought sensitivities of the NPP_M are larger than those of the NPP_S. In tropical forests and extratropical humid regions, the NPP_M also shows significant sensitivity to the SPEI3 over the past three decades, whereas the NPP_S does not (Figures 4b and S3).

Globally, the signs of the correlation coefficients are consistent across most vegetated land areas except for certain tropical forests (Figures 5a and 5b). The NPP_S is significantly and positively correlated with the SPEI3 in 31.6% of vegetated land areas ($p < 0.05$), particularly in arid and semiarid regions. However, the NPP_M is significantly and positively correlated with the SPEI3 in 71.0% of vegetated land areas ($p < 0.05$). In over 95.2% of the vegetated land areas, the correlation coefficients between the NPP_M and SPEI3 are higher than that between the NPP_S and SPEI3 (Figure 5c). In the five climatic regions, the NPP_S and NPP_M values indicate that the NPP in drier areas is more tightly linked to drought conditions (Figure 5d). For example, the NPP_S (NPP_M) in 72.3% (92.2%) of the arid vegetated regions is significantly and positively correlated with the SPEI3. However, the NPP_S (NPP_M) in only 10.7% (52.2%) of the extratropical humid vegetated regions is significantly and positively correlated with the SPEI3.

The signs of drought sensitivity in the NPP_S and NPP_M are consistent across approximately 62.2% of the vegetated land areas (Figures 6a and 6b). However, the NPP_M has stronger drought sensitivity than the NPP_S over 86.4% of vegetated land areas, especially in semiarid regions, such as eastern Australia, southern North America, central Eurasia, and Argentina (Figure 6c). On average, the drought sensitivity of the NPP_S (6.7 gC m^{-2} yr^{-1} or 2% per year) is only one seventh that of the NPP_M (48.3 gC m^{-2} yr^{-1} or 18.8% per

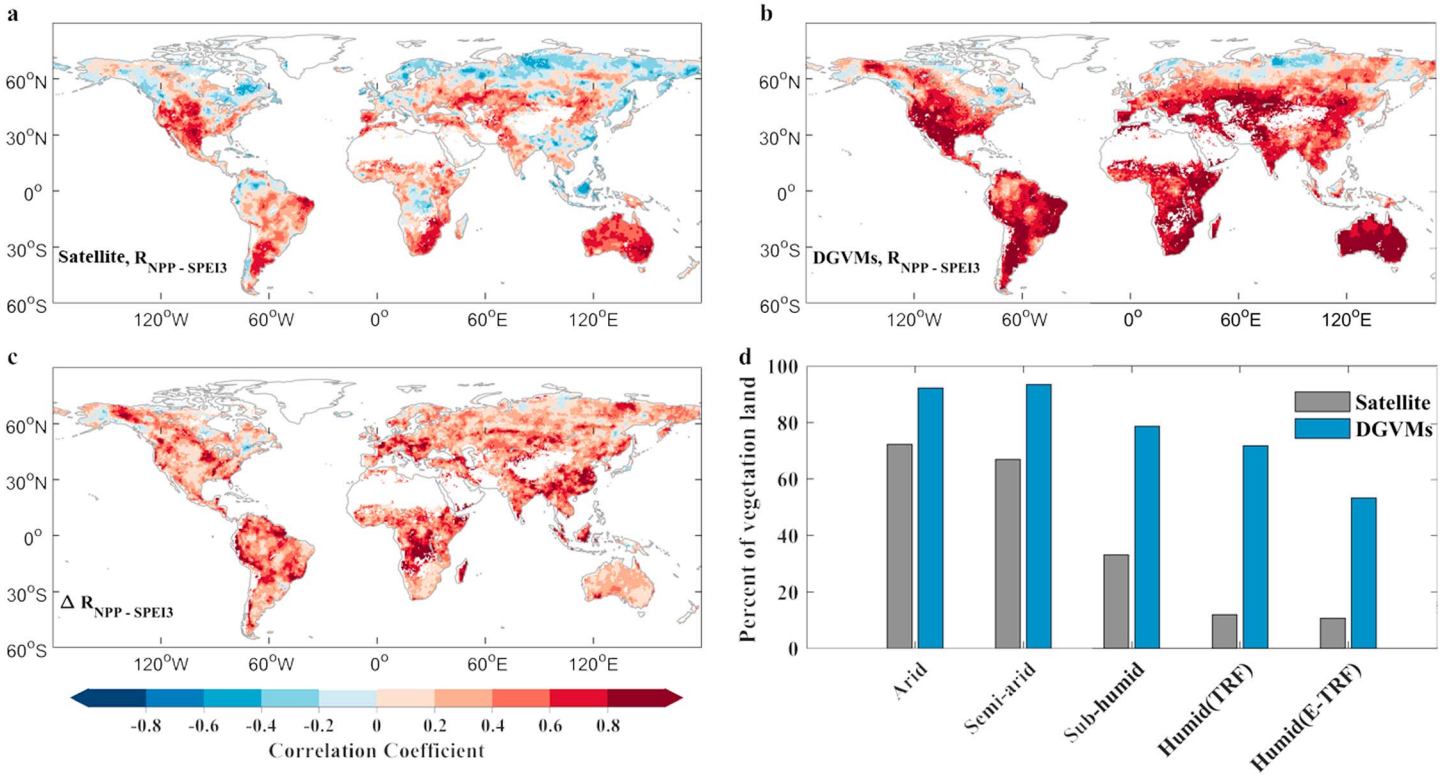

Figure 5. Spatial distributions of the Pearson correlation coefficient between the SPEI3 and (a) NPP_S and (b) NPP_M and (c) their differences (NPP_M-NPP_S). Regions with sparse vegetation were masked in white. (d) Percentage of vegetated land areas in different climatic regions that show significant correlations between the NPP and SPEI values ($p < 0.05$). The gray and blue bars represent the NPP_S and NPP_M estimates, respectively.

year). The frequency distributions of the drought sensitivity of the NPP_M and NPP_S further indicate the higher drought sensitivity of the NPP_M (Figure 6d).

Interestingly, we found that the NPP_M and NPP_S in semiarid regions show the largest sensitivity to SPEI3 variations (Figures 6a and 6b). To further explore the changes in the drought sensitivity of NPP across climatic aridity gradients, we averaged the drought sensitivity at grid level by bins of the aridity index (each interval size of 0.1). An obviously unimodal distribution emerged, and it showed that the NPP drought sensitivity peaked in the semiarid regions ($0.2 < AI < 0.5$; Figure 7), which suggests that the changes in the sensitivity of NPP to the SPEI3 across the climatic aridity gradient are consistent between the NPP_S and NPP_M. In addition, the increasing rate of NPP drought sensitivity in arid regions to the peak values at semiarid regions is approximately 5 to 7 times larger than the decline in NPP sensitivity from semiarid to humid regions. This finding also illustrates the rapidly shifting rates of the NPP drought sensitivity across the climatic aridity gradient.

3.4. Spatial Correlation Between NPP Trends and Drought Trends

The significant and positive correlation between the NPP and SPEI3 trends ($p < 0.01$) suggests that stronger (weaker) annual drought severity could decrease (increase) the annual NPP (Figure 8). This consistent relationship for both the NPP_S and NPP_M indicates that the annual drought severity is an important driver of NPP change. However, the slope of the linear regression between the NPP_M trends and SPEI3 trends (54.1 gC m^{-2} yr^{-2} or 18.6% yr^{-2}) is approximately 9 times higher than that between the NPP_S trends and SPEI3 trends (5.8 gC m^{-2}·yr^{-2} or 2.7% yr^{-2}; Figure 8). Additionally, we found that a significantly linear relationship between the NPP trends and SPEI3 trends occurred across all regions. It is notable that the slope of NPP trends to SPEI3 trends is also largest in the semiarid regions and presents values of 15.5 gC m^{-2} yr^{-2} (NPP_S) and 70.1 gC m^{-2} yr^{-2} (NPP_M; Figures S4 and S5). However, for all climatic regions, the slopes between

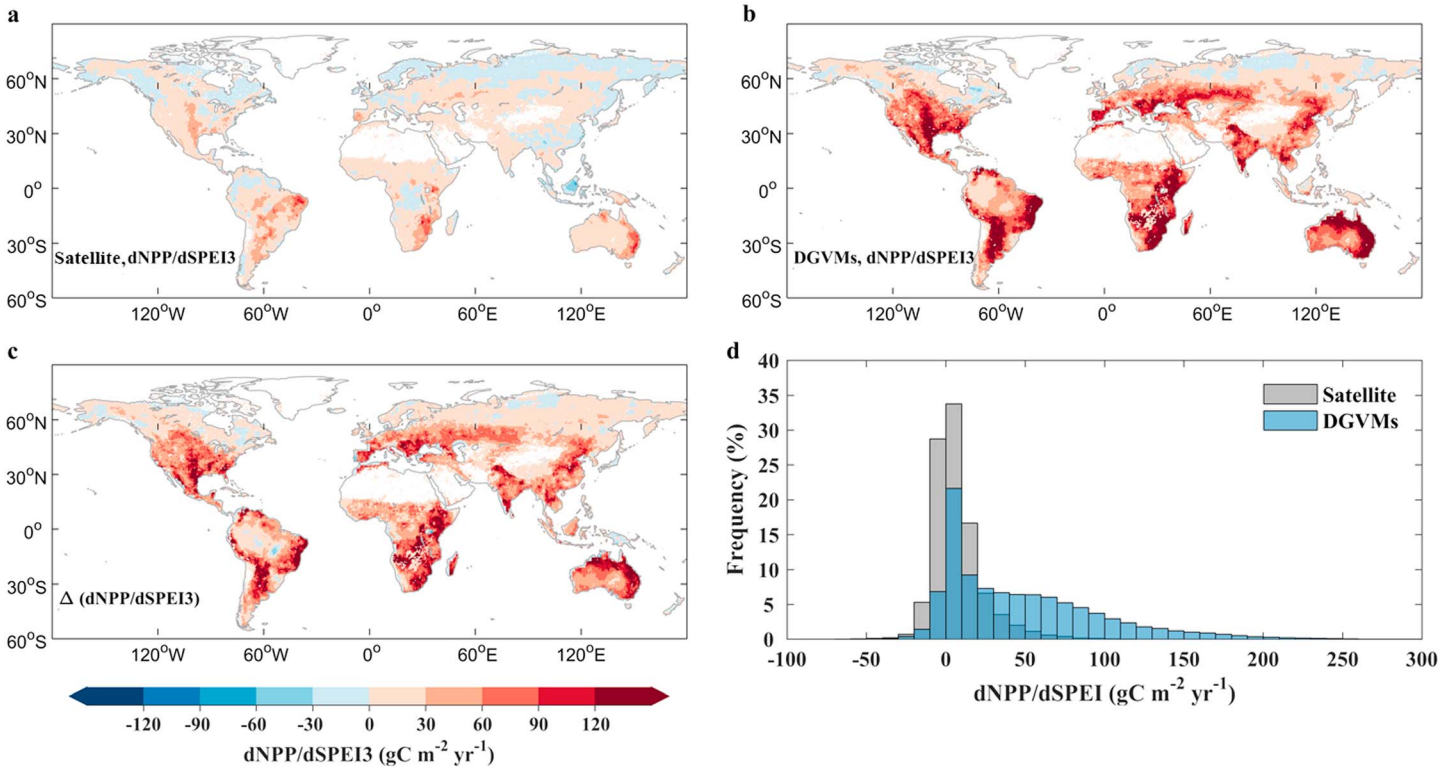

Figure 6. Spatial distributions of the sensitivity of the (a) NPP_S and (b) NPP_M to the SPEI3 and (c) their differences (NPP_M-NPP_S). Regions with sparse vegetation are masked in white. (d) Frequency distribution of the drought sensitivity of the NPP_S (gray) and NPP_M (blue).

the NPP_M trends and SPEI3 trends are still larger than the corresponding slope between the NPP_S trends and SPEI3 trends.

Further, to test the robustness of results, we also used the NDVI and FAPAR as the proxy of vegetation productivity, used the scPDSI and six-month SPEI instead of the SPEI3, and used additional two bin widths of aridity values (0.05 and 0.025), resulting similar results (Figures S6–S15).

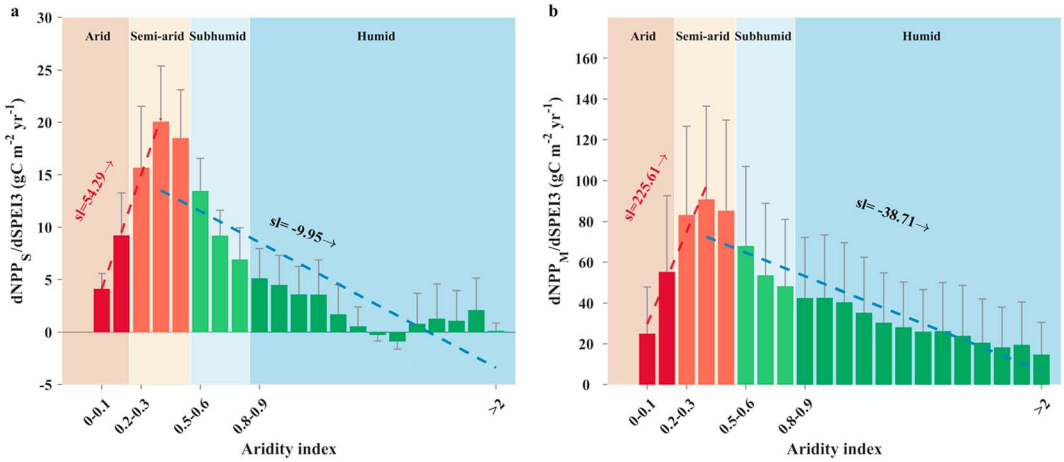

Figure 7. Sensitivity of the (a) NPP_S and (b) NPP_M to the SPEI3 across different climatic conditions. The pixel values over the land vegetation areas were averaged over aridity index values (with 0.1 bins). Vertical color bars indicate the sensitivity of the NPP_S and NPP_M to drought. Error bars indicate the uncertainty caused by model variability and model parameterization for satellite estimates. The dashed lines represent the linear regressions of drought sensitivity versus aridity values from arid to semiarid (red) and semiarid to humid regions (blue). The sl values indicate the regression coefficients of drought sensitivity versus the aridity index.

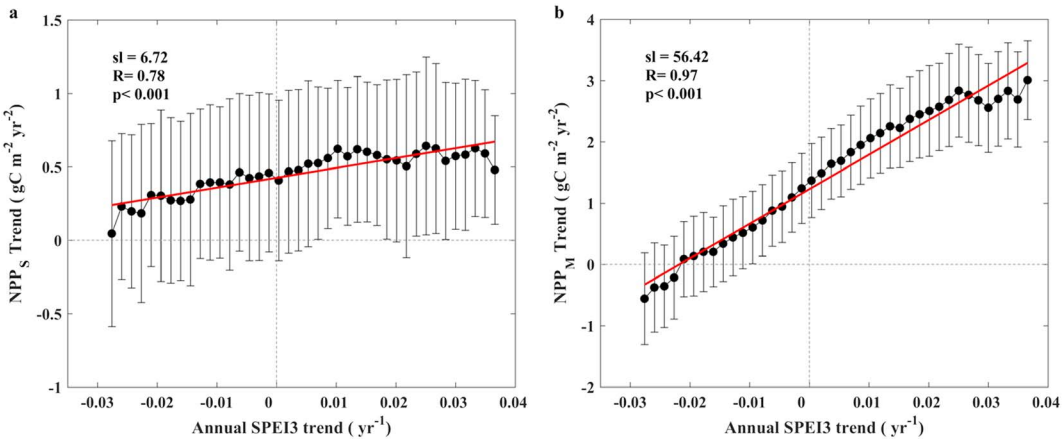

Figure 8. Correlations between the SPEI3 trends and (a) NPP_S and (b) NPP_M trends from 1982 to 2011. The grid values (NPP trends) were averaged by bins of the SPEI3 trends (each interval size of 0.002). Each point in the figure corresponds to the mean of NPP trends within the same SPEI3 trend bin. Error bars show half standard deviation of grid values (NPP trends) in each SPEI3 trend bin. The solid lines represent the linear regressions of NPP trends versus SPEI3 trends. The sl values indicate the regression coefficients. The *R* values show the correlation coefficients between the SPEI3 trends and the NPP_S or NPP_M trends.

4. Discussion

4.1. Response of NPP to Drought Over Different Climatic Regions

Our results show that the sign of the response of NPP_S and NPP_M to SPEI3 is positive over most vegetated land areas during 1982–2011. In particular, the NPP_M and NPP_S are significantly coupled with the SPEI3 in arid, semiarid, and subhumid regions because water availability is the limiting factor for vegetation growth in these regions (Beer et al., 2010; Liu et al., 2018; Nemani et al., 2003). Both the NPP_S and NPP_M are less correlated with drought in most cold humid regions, which may be attributed to a more important role of temperature in explaining NPP variability (Chen et al., 2013; Huang et al., 2016).

Moreover, we found that the drought sensitivity of NPP is highest in semiarid regions in both the DGVMs and satellite models but relatively lower in arid and humid regions. Cleveland et al. (2015) found that semiarid ecosystems in Australia are the most sensitive to drought variations based on the satellite-derived enhanced vegetation index. This could be linked with that the abnormally high precipitation in 2011 enhanced semiarid vegetation growth in the Southern Hemisphere and contributed to more than 60% of the global carbon uptake in 2011 (Poulter et al., 2014). This peak NPP drought sensitivity in semiarid regions also adds to the argument that semiarid vegetation plays a significant role in the regulation of the global carbon cycle (Ahlström et al., 2015; Poulter et al., 2014). By contrast, in arid regions, the drought response of NPP may be constrained by low plant density, leaf area, and highly adapted strategies to water deficits (Chaves et al., 2003; Knapp & Smith, 2001). In humid regions, vegetation is less affected by drought due to higher soil water storage and large and frequent precipitation events (Vicente-Serrano et al., 2013). Under the Representative Concentration Pathway 8.5 scenario, the area of semiarid regions is projected to expand to 20.3% of the global land surface by 2100 (Huang et al., 2017). Consequently, larger areas are expected to become more sensitive to drought in the future, which could increase the vulnerability of the terrestrial carbon cycle to drought in a warming world. In addition, the rising atmospheric CO_2 (CO_2 fertilization) is well known to have positive effects on vegetation growth (Piao et al., 2013; Sitch et al., 2008), while the drought events lasting several months are expected to have the negative effects. On the annual time step, our results indicate that decreasing annual drought severity (i.e., less dry) is significantly correlated with the increasing NPP_S or NPP_M trends during 1982–2011. This finding highlights the strong link between annual water availability and NPP trends and implies that annual drought severity is a key driver of increasing NPP trends, which is consistent with a recent study (Murray-Tortarolo et al., 2016).

4.2. Discrepancies in the Response of the NPP to Drought Between Satellite Models and DGVMs

Despite the consistent drought response signs of the NPP_S and NPP_M across a large proportion of vegetated land areas, we found that the NPP_M is generally more sensitive to drought than NPP_S (Figures 4–8), which is

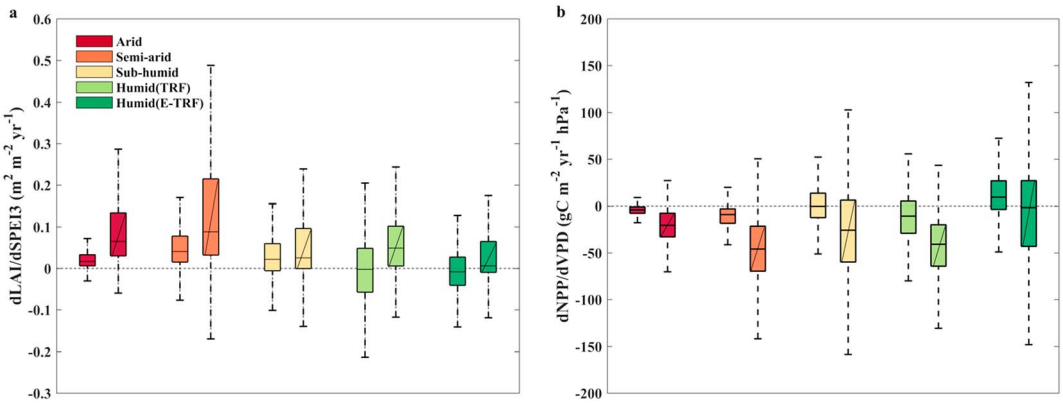

Figure 9. Box plot of the (a) sensitivity of the LAI_O and LAI_M to the SPEI3 and (b) sensitivity of the NPP_S and NPP_M to the VPD in five different climatic regions. Boxes with hatching refer to the NPP_M. Horizontal lines in box plots show the 95th, 75th, 50th, 25th, and 5th percentiles from the top to the bottom.

consistent with the result of a recent study in which drought was shown to cause an approximately 6 times larger reduction of CMIP5 model-derived GPP compared with observation-based GPP globally (Huang et al., 2016). Liu et al. (2017) found that CMIP5 NPP is oversensitive to seasonal precipitation variations relative to satellite NPP. Piao et al. (2013) also found that GPP from models is more sensitive to precipitation than data-oriented GPP across biomes and globally. Substituting the SPEI with precipitation, we also found that the NPP_M has a positive apparent sensitivity to precipitation ($p < 0.05$) while the NPP_S presents an insignificant sensitivity to precipitation ($p > 0.05$) following the method outlined in Piao et al. (2013).

Considering the mechanisms related to the drought response of the NPP in the light-use efficiency model used to derive the NPP_S, the following two important mechanisms may directly determine the drought sensitivity of NPP_S: the sensitivity of the LAI to drought and the sensitivity of NPP to the VPD (Zhao & Running, 2010). We then investigated the drought sensitivity of the LAI between satellites and models and the sensitivity of NPP to VPD as observed with the NPP_S and derived by DGVMs to explain the higher drought sensitivity of the NPP_M than the NPP_S. Indeed, higher drought sensitivities of the LAI_M are observed across five climatic regions (Figures 9a and S16c). Both NPP_S and NPP_M are regulated by LAI through the amount of leaf carry out photosynthesis. The larger drought sensitivity of LAI_M partly explains the discrepancies between the drought sensitivity of NPP_S and NPP_M. The analysis of LAI-drought relationship provides complementary evidence to our results based on NPP, since satellite-derived LAI does not rely on the light-use efficiency model used in NPP_S. This finding is consistent with a recent global analysis, which also shows a similar oversensitivity to drought in the CMIP5-derived LAI compared with the satellite-derived LAI (Huang et al., 2016). The oversensitivity may be improved through validating the parametrization that affect LAI (including leaf carbon allocation and turnover under drought). DGVMs may need to constrain the reduction of LAI under water stress. Similarly, the NPP_M is more sensitive to the VPD (Figures 9b and S16f), thus indicating that an equivalent increase in the VPD will produce a greater decrease in NPP_M than NPP_S. The VPD is used in both the DGVMs and satellite retrievals to constrain NPP under water stress (De Kauwe et al., 2013; Zhao & Running, 2010). The VPD is a critical parameter for modeling stomatal conductance in many DGVMs (Cowan & Farquhar, 1977; De Kauwe et al., 2013) and significantly affects gas, water, and carbon exchange (Novick et al., 2016). The higher NPP drought sensitivities in the DGVMs than in satellite products can be attributed to the different sensitivities of the NPP or stomatal conductance to the VPD in the DGVMs and satellites products.

4.3. Perspectives on the NPP Response to Drought in Models

We attempted to derive the sensitivity of NPP to drought via satellite models and DGVMs; however, our study presented some uncertainties. Satellite FAPAR and LAI, which were used as the input data for the NPP_S, may be affected by cloud and aerosol contamination in tropical forests (Hilker et al., 2014; Zhou et al., 2014), and less reliable climate observations were available in tropic regions for use as input data for the model. The simulated plant physiological responses present large uncertainties in DGVMs in tropical forests (Huntingford et al., 2013). A recent study in tropical forests reported that NPP estimates from plot-based

measurements, satellites, and terrestrial ecosystem models presented considerable temporal and spatial variations (Cleveland et al., 2015). In addition, Powell et al. (2013) found that five current models could not accurately simulate the response of ecosystem to drought in the Amazon. Therefore, the response of NPP to drought in tropical forests requires further ground studies. The effects of landscape changes are not considered and could bring biases to some locations in our analysis. Note that since FAPAR and NDVI are transformations of the same input data, although nonlinearities might arise, they could not be treated as separate strictly. It should also be noted that DGVMs and the MODIS algorithm do not share common meteorological drivers and that this difference may have the potential to bring biases to the analysis.

Additionally, uncertainties were observed in the characterization of the NPP responses to water stress in both the satellite models and DGVMs. Satellite NPP relies heavily on vegetation indices, such as NDVI and FAPAR, to monitor vegetation state; however, the highly heterogeneous dryland ecosystem may show low spectral sensitivity to drought, which could underestimate the drought sensitivity of satellite NPP in drylands (Biederman et al., 2017; Smith et al., 2018). Moreover, although atmospheric moisture demand greatly impacts ecosystem carbon and water fluxes (Novick et al., 2016), soil moisture stress can also represent environmental water stress because soil moisture is the direct pool of water to support vegetation growth. However, the MODIS algorithm only considers the VPD effects and does not consider the soil moisture stress, which could affect the estimation of the drought sensitivity of NPP (Zhao & Running, 2010). Efforts are needed to incorporate the effects of soil moisture into satellite models. The DGVMs consider the constraints of soil moisture stress and VPD stress on NPP, which benefited the simulated response of NPP to drought. Yet DGVMs may present inconsistencies in the limiting role of soil moisture and VPD on stomatal conductance and its relationship with the assimilation rate and water use efficiency, which can affect vegetation photosynthesis (Egea et al., 2011). For instance, most models, such as CABLE, CLM4, ISAM, LPJ-GUESS, O-CN, SDVGM, and TECO, used different version of the stomatal conductance model of Ball, Berry, and Leuning (De Kauwe et al., 2013). Modelers should consider validating the model formulations against in situ observations, especially the sensitivity of stomatal conductance to VPD. Moreover, terrestrial ecosystem models are also highly sensitive to the parameterization of plant root characteristics, such as the rooting depth and rooting distribution. A lack of knowledge of rooting characteristics limits our ability to simulate vegetation dynamics under water stress in models (Feddes et al., 2001; Kleidon & Heimann, 1998). Previous studies have reported that the limited legacy or lagged effects of drought on terrestrial ecosystem production could be simulated by current models (Anderegg et al., 2015). The CO_2 fertilization effects are not thoroughly considered in the MODIS algorithm, which could cause higher drought sensitivity of satellite-derived NPP (De Kauwe et al., 2016). These uncertainties should be further investigated to decrease the model biases in simulated drought impacts on terrestrial ecosystems. It is also useful to compare the drought sensitivity of NPP from satellite models or DGVMs with that measured on sites. On the site scale, the measured NPP is generally dominated by one plant functional type. But several different plant functional types are aggregated to one grid cell in the NPP_S or NPP_M, and the area of one grid cell (0.5°) is much larger than the site area. Thus, it is suggested to conduct model simulations or apply the satellite model on the site scale in further study. Especially, the model simulations should follow the standardized initialization and drought simulation protocol (Powell et al., 2013; Wu et al., 2018). In addition, the time duration of most available sites is not long enough to detect the impacts of some extreme drought events (e.g., a drought event occurs once in 30 years) on NPP. We still need long-term observations to benchmark the drought sensitivity of NPP.

5. Conclusions

In summary, we investigated regional and global NPP drought response derived from satellites and eight DGVMs for the period 1982–2011.Our results indicate that the sign of NPP's response to drought is consistent across satellite-derived NPP and DGVM-derived NPP over most vegetated land areas. Moreover, both the drought sensitivity of satellite-derived NPP and DGVM-derived NPP show a unimodal distribution across climatic gradients, with peak drought sensitivity observed in semiarid regions. It states that NPP in semiarid regions is most sensitive to drought variations and it could be related to the moderate plant density and lowly adapted strategies to water deficits in semiarid regions. In addition, stronger (weaker) annual drought severity could decrease (increase) the annual satellite-derived NPP or DGVM-derived NPP globally during 1982–2011. However, the DGVM-derived NPP is more sensitive to drought than the satellite-derived NPP,

which could be caused by the higher drought sensitivity of the simulated LAI and the overresponse of the DGVM-derived NPP to VPD. Therefore, combining long-term in situ observations, manipulative ecosystem experiments, satellite observations, and models is encouraged to provide insights on the mechanisms that explain the discrepancies in the drought response of NPP between satellite models and DGVMs.

Acknowledgments

Data used are available at https://ecocast.arc.nasa.gov/data/pub/gimms/3g.v1/ (GIMMS NDVI3g v1), http://sites.bu.edu/cliveg/files/2014/08/gimms_list.txt (GIMMIS LAI3g and FPAR3g), http://digital.csic.es/handle/10261/128892 (SPEI), https://crudata.uea.ac.uk/cru/data/drought/ (scPDSI), and https://lpdaac.usgs.gov/data_access/data_pool (MCD12C1). We thank the TRENDY project and TRENDY modelers for contributing the model outputs. We thank William Kolby for providing the long-term satellite NPP data sets. We would like to thank the editors and reviewers for their insight comments and suggestions on the manuscript. This study was supported by the National Basic Research Program of China (grant 2015CB452702). The authors have no conflicts of interest to declare.

References

AghaKouchak, A., Farahmand, A., Melton, F. S., Teixeira, J., Anderson, M. C., Wardlow, B. D., & Hain, C. R. (2015). Remote sensing of drought: Progress, challenges and opportunities. *Reviews of Geophysics*, *53*, 452–480. https://doi.org/10.1002/2014RG000456

Ahlström, A., Raupach, M. R., Schurgers, G., Smith, B., Arneth, A., Jung, M., & Jain, A. K. (2015). Carbon cycle. The dominant role of semi-arid ecosystems in the trend and variability of the land CO_2 sink. *Science*, *348*(6237), 895–899. https://doi.org/10.1126/science.aaa1668

Anderegg, W. R., Schwalm, C., Biondi, F., Camarero, J. J., Koch, G., Litvak, M., & Williams, A. (2015). Pervasive drought legacies in forest ecosystems and their implications for carbon cycle models. *Science*, *349*(6247), 528–532. https://doi.org/10.1126/science.aab1833

Barman, R., Jain, A. K., & Liang, M. L. (2014). Climate-driven uncertainties in modeling terrestrial gross primary production: A site level to global-scale analysis. *Global Change Biology*, *20*(5), 1394–1411. https://doi.org/10.1111/gcb.12474

Beer, C., Reichstein, M., Tomelleri, E., Ciais, P., Jung, M., Carvalhais, N., et al. (2010). Terrestrial gross carbon dioxide uptake: Global distribution and covariation with climate. *Science*, *329*(5993), 834–838. https://doi.org/10.1126/science.1184984

Beguería, S., Vicente-Serrano, S. M., Reig, F., & Latorre, B. (2014). Standardized precipitation evapotranspiration index (SPEI) revisited: Parameter fitting, evapotranspiration models, tools, datasets and drought monitoring. *International Journal of Climatology*, *34*(10), 3001–3023. https://doi.org/10.1002/joc.3887

Biederman, J. A., Scott, R. L., Bell, T. W., Bowling, D. R., Dore, S., Garatuza-Payan, J., et al. (2017). CO_2 exchange and evapotranspiration across dryland ecosystems of southwestern North America. *Global Change Biology*, *23*(10), 4204–4221. https://doi.org/10.1111/gcb.13686

Chaves, M. M., Maroco, J. P., & Pereira, J. S. (2003). Understanding plant responses to drought—From genes to the whole plant. *Functional Plant Biology*, *30*(3), 239–264. https://doi.org/10.1071/FP02076

Chen, T., Werf, G. R., Jeu, R. A. M., Wang, G., & Dolman, A. J. (2013). A global analysis of the impact of drought on net primary productivity. *Hydrology and Earth System Sciences*, *17*(10), 3885–3894. https://doi.org/10.5194/hess-17-3885-2013

Ciais, P., Reichstein, M., Viovy, N., Granier, A., Ogée, J., Allard, V., et al. (2005). Europe-wide reduction in primary productivity caused by the heat and drought in 2003. *Nature*, *437*(7058), 529–533. https://doi.org/10.1038/nature03972

Cleveland, C. C., Taylor, P., Chadwick, K. D., Dahlin, K., Doughty, C. E., Malhi, Y., et al. (2015). A comparison of plot-based satellite and Earth system model estimates of tropical forest net primary production. *Global Biogeochemical Cycles*, *29*, 626–644. https://doi.org/10.1002/2014GB005022

Cowan, I., & Farquhar, G. (1977). Stomatal function in relation to leaf metabolism and environment. Paper presented at the Symposia of the Society for Experimental Biology.

De Kauwe, M. G., Keenan, T. F., Medlyn, B. E., Prentice, I. C., & Terrer, C. (2016). Satellite based estimates underestimate the effect of CO_2 fertilization on net primary productivity. *Nature Climate Change*, *6*(10), 892–893. https://doi.org/10.1038/nclimate3105

De Kauwe, M. G., Medlyn, B. E., Zaehle, S., Walker, A. P., Dietze, M. C., Hickler, T., et al. (2013). Forest water use and water use efficiency at elevated CO_2: A model-data intercomparison at two contrasting temperate forest FACE sites. *Global Change Biology*, *19*(6), 1759–1779. https://doi.org/10.1111/gcb.12164

Eamus, D., Boulain, N., Cleverly, J., & Breshears, D. D. (2013). Global change-type drought-induced tree mortality: Vapor pressure deficit is more important than temperature per se in causing decline in tree health. *Ecology and Evolution*, *3*(8), 2711–2729. https://doi.org/10.1002/ece3.664

Egea, G., Verhoef, A., & Vidale, P. L. (2011). Towards an improved and more flexible representation of water stress in coupled photosynthesis–stomatal conductance models. *Agricultural and Forest Meteorology*, *151*(10), 1370–1384. https://doi.org/10.1016/j.agrformet.2011.05.019

El-Masri, B., Barman, R., Meiyappan, P., Song, Y., Liang, M. L., & Jain, A. K. (2013). Carbon dynamics in the Amazonian basin: Integration of eddy covariance and ecophysiological data with a land surface model. *Agricultural and Forest Meteorology*, *182-183*, 156–167. https://doi.org/10.1016/j.agrformet.2013.03.011

Feddes, R. A., Hoff, H., Bruen, M., Dawson, T., de Rosnay, P., Dirmeyer, O., et al. (2001). Modeling root water uptake in hydrological and climate models. *Bulletin of the American Meteorological Society*, *82*(12), 2797–2809. https://doi.org/10.1175/1520-0477(2001)082<2797:MRWUIH>2.3.CO;2

Field, C. B., Behrenfeld, M. J., Randerson, J. T., & Falkowski, P. (1998). Primary production of the biosphere: Integrating terrestrial and oceanic components. *Science*, *281*(5374), 237–240. https://doi.org/10.1126/science.281.5374.237

Frank, D., Reichstein, M., Bahn, M., Thonicke, K., Frank, D., Mahecha, M. D., et al. (2015). Effects of climate extremes on the terrestrial carbon cycle: Concepts, processes and potential future impacts. *Global Change Biology*, *21*(8), 2861–2880. https://doi.org/10.1111/gcb.12916

Haberl, H., Erb, K. H., Krausmann, F., Gaube, V., Bondeau, A., Plutzar, C., et al. (2007). Quantifying and mapping the human appropriation of net primary production in Earth's terrestrial ecosystems. *Proceedings of the National Academy of Sciences*, *104*(31), 12,942–12,947. https://doi.org/10.1073/pnas.0704243104

Harris, I., Jones, P., Osborn, T., & Lister, D. (2014). Updated high-resolution grids of monthly climatic observations—The CRU TS3.10 dataset. *International Journal of Climatology*, *34*(3), 623–642. https://doi.org/10.1002/joc.3711

Hilker, T., Lyapustin, A. I., Tucker, C. J., Hall, F. G., Myneni, R. B., Wang, Y., et al. (2014). Vegetation dynamics and rainfall sensitivity of the Amazon. *Proceedings of the National Academy of Sciences of the United States of America*, *111*(45), 16,041–16,046. https://doi.org/10.1073/pnas.1404870111

Hoover, D. L., & Rogers, B. M. (2016). Not all droughts are created equal: The impacts of interannual drought pattern and magnitude on grassland carbon cycling. *Global Change Biology*, *22*(5), 1809–1820. https://doi.org/10.1111/gcb.13161

Huang, J., Li, Y., Fu, C., Chen, F., Fu, Q., Dai, A., et al. (2017). Dryland climate change: Recent progress and challenges. *Reviews of Geophysics*, *55*, 719–778. https://doi.org/10.1002/2016rg000550

Huang, Y. Y., Gerber, S., Huang, T. Y., & Lichstein, J. W. (2016). Evaluating the drought response of CMIP5 models using global gross primary productivity, leaf area, precipitation, and soil moisture data. *Global Biogeochemical Cycles*, *30*, 1827–1846. https://doi.org/10.1002/2016GB005480

Huntingford, C., Zelazowski, P., Galbraith, D., Mercado, L. M., Sitch, S., Fisher, R., et al. (2013). Simulated resilience of tropical rainforests to CO_2-induced climate change. *Nature Geoscience*, *6*(4), 268–273. https://doi.org/10.1038/ngeo1741

Jiang, X. Y., Rauscher, S. A., Ringler, T. D., Lawrence, D. M., Williams, A. P., Allen, C. D., et al. (2013). Projected future changes in vegetation in Western North America in the twenty-first century. *Journal of Climate*, *26*(11), 3671–3687. https://doi.org/10.1175/JCLI-D-12-00430.1

Jung, M., Reichstein, M., Schwalm, C. R., Huntingford, C., Sitch, S., Ahlstrom, A., et al. (2017). Compensatory water effects link yearly global land CO_2 sink changes to temperature. *Nature*, *541*(7638), 516–520. https://doi.org/10.1038/nature20780

Kleidon, A., & Heimann, M. (1998). A method of determining rooting depth from a terrestrial biosphere model and its impacts on the global water and carbon cycle. *Global Change Biology*, *4*(3), 275–286. https://doi.org/10.1046/j.1365-2486.1998.00152.x

Knapp, A. K., & Smith, M. D. (2001). Variation among biomes in temporal dynamics of aboveground primary production. *Science*, *291*(5503), 481–484. https://doi.org/10.1126/science.291.5503.481

Lawrence, D. M., Oleson, K. W., Flanner, M. G., Thornton, P. E., Swenson, S. C., Lawrence, P. J., et al. (2011). Parameterization improvements and functional and structural advances in version 4 of the Community Land Model. *Journal of Advances in Modeling Earth Systems*, *3*, M03001. https://doi.org/10.1029/2011MS000045

Le Quéré, C., Andrew, R. M., Canadell, J. G., Sitch, S., Korsbakken, J. I., Peters, G. P., et al. (2016). Global carbon budget 2016. *Earth System Science Data*, *8*(2), 605–649. https://doi.org/10.5194/essd-8-605-2016

Liu, L. B., Zhang, Y. T., Wu, S. Y., Li, S. C., & Qin, D. H. (2018). Water memory effects and their impacts on global vegetation productivity and resilience. *Scientific Reports*, *8*. https://doi.org/10.1038/s41598-018-21339-4

Liu, Y. W., Piao, S. L., Lian, X., Ciais, P., & Smith, W. K. (2017). Seasonal responses of terrestrial carbon cycle to climate variations in CMIP5 models: Evaluation and projection. *Journal of Climate*, *30*(16), 6481–6503. https://doi.org/10.1175/JCLI-D-16-0555.1

Ma, X., Huete, A., Moran, S., Ponce-Campos, G., & Eamus, D. (2015). Abrupt shifts in phenology and vegetation productivity under climate extremes. *Journal of Geophysical Research: Biogeosciences*, *120*, 2036–2052. https://doi.org/10.1002/2015JG003144

Murray-Tortarolo, G., Friedlingstein, P., Sitch, S., Seneviratne, S. I., Fletcher, I., Mueller, B., et al. (2016). The dry season intensity as a key driver of NPP trends. *Geophysical Research Letters*, *43*, 2632–2639. https://doi.org/10.1002/2016gl068240

Nemani, R. R., Keeling, C. D., Hashimoto, H., Jolly, W. M., Piper, S. C., Tucker, C. J., et al. (2003). Climate-driven increases in global terrestrial net primary production from 1982 to 1999. *Science*, *300*(5625), 1560–1563. https://doi.org/10.1126/science.1082750

Norby, R. J., Warren, J. M., Iversen, C. M., Medlyn, B. E., & McMurtrie, R. E. (2010). CO_2 enhancement of forest productivity constrained by limited nitrogen availability. *Proceedings of the National Academy of Sciences*, *107*(45), 19,368–19,373. https://doi.org/10.1073/pnas.1006463107

Novick, K. A., Ficklin, D. L., Stoy, P. C., Williams, C. A., Bohrer, G., Oishi, A. C., et al. (2016). The increasing importance of atmospheric demand for ecosystem water and carbon fluxes. *Nature Climate Change*, *6*(11), 1023–1027. https://doi.org/10.1038/nclimate3114

Oleson, K. W., Lawrence, D. M., Bonan, G. B., Flanner, M. G., Kluzek, E., Lawrence, P. J., et al. (2010). Technical description of version 4.0 of the Community Land Model (CLM).

Peel, M. C., Finlayson, B. L., & Mcmahon, T. A. (2007). Updated world map of the Köppen-Geiger climate classification. *Hydrology and Earth System Sciences*, *4*(2), 439–473. https://doi.org/10.5194/hessd-4-439-2007

Peng, S., Piao, S., Ciais, P., Myneni, R. B., Chen, A., Chevallier, F., et al. (2013). Asymmetric effects of daytime and night-time warming on northern hemisphere vegetation. *Nature*, *501*(7465), 88–92. https://doi.org/10.1038/nature12434

Piao, S., Sitch, S., Ciais, P., Friedlingstein, P., Peylin, P., Wang, X., et al. (2013). Evaluation of terrestrial carbon cycle models for their response to climate variability and to CO_2 trends. *Global Change Biology*, *19*(7), 2117–2132. https://doi.org/10.1111/gcb.12187

Poulter, B., Frank, D., Ciais, P., Myneni, R. B., Andela, N., Bi, J., et al. (2014). Contribution of semi-arid ecosystems to interannual variability of the global carbon cycle. *Nature*, *509*(7502), 600–603. https://doi.org/10.1038/nature13376

Powell, T. L., Galbraith, D. R., Christoffersen, B. O., Harper, A., Imbuzeiro, H. M. A., Rowland, L., et al. (2013). Confronting model predictions of carbon fluxes with measurements of Amazon forests subjected to experimental drought. *New Phytologist*, *200*(2), 350–365. https://doi.org/10.1111/nph.12390

Raddatz, T. J., Reick, C. H., Knorr, W., Kattge, J., Roeckner, E., Schnur, R., et al. (2007). Will the tropical land biosphere dominate the climate-carbon cycle feedback during the twenty-first century? *Climate Dynamics*, *29*(6), 565–574. https://doi.org/10.1007/s00382-007-0247-8

Reichstein, M., Bahn, M., Ciais, P., Frank, D., Mahecha, M. D., Seneviratne, S. I., et al. (2013). Climate extremes and the carbon cycle. *Nature*, *500*(7462), 287–295. https://doi.org/10.1038/nature12350

Running, S. W. (2012). Ecology. A measurable planetary boundary for the biosphere. *Science*, *337*(6101), 1458–1459. https://doi.org/10.1126/science.1227620

Running, S. W., Nemani, R. R., Heinsch, F. A., Zhao, M. S., Reeves, M., & Hashimoto, H. (2004). A continuous satellite-derived measure of global terrestrial primary production. *Bioscience*, *54*(6), 547–560. https://doi.org/10.1641/0006-3568(2004)054[0547:ACSMOG]2.0.CO;2

Schimel, D., Stephens, B. B., & Fisher, J. B. (2015). Effect of increasing CO_2 on the terrestrial carbon cycle. *Proceedings of the National Academy of Sciences of the United States of America*, *112*(2), 436–441. https://doi.org/10.1073/pnas.1407302112

Schrier, G., Barichivich, J., Briffa, K., & Jones, P. (2013). A scPDSI-based global data set of dry and wet spells for 1901–2009. *Journal of Geophysical Research: Atmospheres*, *118*, 4025–4048. https://doi.org/10.1002/jgrd.50355

Sitch, S., Friedlingstein, P., Gruber, N., Jones, S., Murray-Tortarolo, G., Ahlström, A., et al. (2015). Recent trends and drivers of regional sources and sinks of carbon dioxide. *Biogeosciences*, *12*(3), 653–679. https://doi.org/10.5194/bg-12-653-2015

Sitch, S., Huntingford, C., Gedney, N., Levy, P., Lomas, M., Piao, S., et al. (2008). Evaluation of the terrestrial carbon cycle, future plant geography and climate-carbon cycle feedbacks using five dynamic global vegetation models (DGVMs). *Global Change Biology*, *14*(9), 2015–2039. https://doi.org/10.1111/j.1365-2486.2008.01626.x

Smith, B., Prentice, I. C., & Sykes, M. T. (2001). Representation of vegetation dynamics in the modelling of terrestrial ecosystems: Comparing two contrasting approaches within European climate space. *Global Ecology and Biogeography, 10*(6), 621–637. https://doi.org/10.1046/j.1466-822X.2001.t01-1-00256.x, https://doi.org/10.1046/j.1466-822X.2001.00256.x

Smith, W. K., Biederman, J. A., Scott, R. L., Moore, D. J. P., He, M., Kimball, J. S., et al. (2018). Chlorophyll fluorescence better captures seasonal and interannual gross primary productivity dynamics across dryland ecosystems of southwestern North America. *Geophysical Research Letters*, *45*, 748–757. https://doi.org/10.1002/2017gl075922

Smith, W. K., Reed, S. C., Cleveland, C. C., Ballantyne, A. P., Anderegg, W. R. L., Wieder, W. R., et al. (2016). Large divergence of satellite and Earth system model estimates of global terrestrial CO_2 fertilization. *Nature Climate Change*, *6*(3), 306–310. https://doi.org/10.1038/Nclimate2879

Smith, W. K., Zhao, M. S., & Running, S. W. (2012). Global bioenergy capacity as constrained by observed biospheric productivity rates. *Bioscience*, *62*(10), 911–922. https://doi.org/10.1525/bio.2012.62.10.11

Stocker, B. D., Roth, R., Joos, F., Spahni, R., Steinacher, M., Zaehle, S., et al. (2013). Multiple greenhouse-gas feedbacks from the land biosphere under future climate change scenarios. *Nature Climate Change*, *3*(7), 666–672. https://doi.org/10.1038/Nclimate1864

Tucker, C. J., Pinzon, J. E., Brown, M. E., Slayback, D. A., Pak, E. W., Mahoney, R., et al. (2005). An extended AVHRR 8-km NDVI dataset compatible with MODIS and SPOT vegetation NDVI data. *International Journal of Remote Sensing*, *26*(20), 4485–4498. https://doi.org/10.1080/01431160500168686

Unesco. (1979). Map of the world distribution of arid regions: Explanatory note: UNESCO.
Vicente-Serrano, S. M., Beguería, S., & López-Moreno, J. I. (2010). A multiscalar drought index sensitive to global warming: The standardized precipitation evapotranspiration index. *Journal of Climate*, *23*(7), 1696–1718. https://doi.org/10.1175/2009JCLI2909.1
Vicente-Serrano, S. M., Gouveia, C., Camarero, J. J., Begueria, S., Trigo, R., Lopez-Moreno, J. I., et al. (2013). Response of vegetation to drought time-scales across global land biomes. *Proceedings of the National Academy of Sciences of the United States of America*, *110*(1), 52–57. https://doi.org/10.1073/pnas.1207068110
Wang, W., Peng, C., Kneeshaw, D. D., Larocque, G. R., & Luo, Z. (2012). Drought-induced tree mortality: Ecological consequences, causes, and modeling. *Environmental Reviews*, *20*(2), 109–121. https://doi.org/10.1139/a2012-004
Wang, Y. P., Kowalczyk, E., Leuning, R., Abramowitz, G., Raupach, M. R., Pak, B., et al. (2011). Diagnosing errors in a land surface model (CABLE) in the time and frequency domains. *Journal of Geophysical Research*, *116*, G01034. https://doi.org/10.1029/2010JG001385
Wang, Y. P., Law, R. M., & Pak, B. (2010). A global model of carbon, nitrogen and phosphorus cycles for the terrestrial biosphere. *Biogeosciences*, *7*(7), 2261–2282. https://doi.org/10.5194/bg-7-2261-2010
Wu, D. H., Ciais, P., Viovy, N., Knapp, A. K., Wilcox, K., Bahn, M., et al. (2018). Asymmetric responses of primary productivity to altered precipitation simulated by ecosystem models across three long-term grassland sites. *Biogeosciences*, *15*(11), 3421–3437. https://doi.org/10.5194/bg-15-3421-2018
Zeng, N., Mariotti, A., & Wetzel, P. (2005). Terrestrial mechanisms of interannual CO(2) variability. *Global Biogeochemical Cycles*, *19*, GB1016. https://doi.org/10.1029/2004GB002273
Zhao, M., & Running, S. W. (2010). Drought-induced reduction in global terrestrial net primary production from 2000 through 2009. *Science*, *329*(5994), 940–943. https://doi.org/10.1126/science.1192666
Zhou, L., Tian, Y., Myneni, R. B., Ciais, P., Saatchi, S., Liu, Y. Y., et al. (2014). Widespread decline of Congo rainforest greenness in the past decade. *Nature*, *509*(7498), 86–90. https://doi.org/10.1038/nature13265
Zhu, Z., Bi, J., Pan, Y., Ganguly, S., Anav, A., Xu, L., et al. (2013). Global data sets of vegetation leaf area index (LAI) 3g and fraction of photosynthetically active radiation (FPAR) 3g derived from global inventory modeling and mapping studies (GIMMS) normalized difference vegetation index (NDVI3g) for the period 1981 to 2011. *Remote Sensing*, *5*(2), 927–948.
Zscheischler, J., Mahecha, M. D., Harmeling, S., & Reichstein, M. (2013). Detection and attribution of large spatiotemporal extreme events in Earth observation data. *Ecological Informatics*, *15*, 66–73. https://doi.org/10.1016/j.ecoinf.2013.03.004
Zscheischler, J., Michalak, A. M., Schwalm, C., Mahecha, M. D., Huntzinger, D. N., Reichstein, M., et al. (2014). Impact of large-scale climate extremes on biospheric carbon fluxes: An intercomparison based on MsTMIP data. *Global Biogeochemical Cycles*, *28*, 585–600. https://doi.org/10.1002/2014GB004826